12-18-2015

Correlations between quantitative fat–water magnetic resonance imaging and computed tomography in human subcutaneous white adipose tissue

Aliya Gifford
Vanderbilt University

Ronald C. Walker
Vanderbilt University

Theodore F. Towse
Grand Valley State University, towset@gvsu.edu

E Brian Welch
Vanderbilt University

Journal of Medical Imaging

MedicalImaging.SPIEDigitalLibrary.org

Correlations between quantitative fat–water magnetic resonance imaging and computed tomography in human subcutaneous white adipose tissue

Aliya Gifford
Ronald C. Walker
Theodore F. Towse
E. Brian Welch

SPIE.

Correlations between quantitative fat–water magnetic resonance imaging and computed tomography in human subcutaneous white adipose tissue

Aliya Gifford,[a,b] Ronald C. Walker,[c,d] Theodore F. Towse,[a,e] and E. Brian Welch[a,d,*]
[a]Vanderbilt University, Institute of Imaging Science, 1161 21st Avenue South, Medical Center North, AA-1105, Nashville, Tennessee 37235, United States
[b]Vanderbilt University, Chemical and Physical Biology Program, 1161 21st Avenue South, Medical Center North, AA 3105, Nashville, Tennessee 37235, United States
[c]Tennessee Valley VA Healthcare, Department of Medical Imaging, 1161 21st Avenue South, Medical Center North, CCC-1121, Nashville, Tennessee 37235, United States
[d]Vanderbilt University, School of Medicine, Department of Radiology and Radiological Sciences, 1161 21st Avenue South, Medical Center North, CCC-1121, Nashville, Tennessee 37235, United States
[e]Vanderbilt University, School of Medicine, Department of Physical Medicine and Rehabilitation, 2201 Children's Way #1014, Nashville, Tennessee 37235, United States

Abstract. Beyond estimation of depot volumes, quantitative analysis of adipose tissue properties could improve understanding of how adipose tissue correlates with metabolic risk factors. We investigated whether the fat signal fraction (FSF) derived from quantitative fat–water magnetic resonance imaging (MRI) scans at 3.0 T correlates to CT Hounsfield units (HU) of the same tissue. These measures were acquired in the subcutaneous white adipose tissue (WAT) at the umbilical level of 21 healthy adult subjects. A moderate correlation exists between MRI- and CT-derived WAT values for all subjects, $R^2 = 0.54$, $p < 0.0001$, with a slope of −2.6, (95% CI [−3.3, −1.8]), indicating that a decrease of 1 HU equals a mean increase of 0.38% FSF. We demonstrate that FSF estimates obtained using quantitative fat–water MRI techniques correlate with CT HU values in subcutaneous WAT, and therefore, MRI-based FSF could be used as an alternative to CT HU for assessing metabolic risk factors. [DOI: 10.1117/1.JMI.2.4.046001]

Keywords: fat quantification; obesity; quantitative biomarker; Hounsfield units; fat signal fraction.

Paper 15121RR received Jun. 15, 2015; accepted for publication Nov. 18, 2015; published online Dec. 18, 2015.

1 Introduction

Quantifying imaging-derived properties of adipose tissue is an important field of research. The presence of adipose tissue can be a factor in many health conditions such as hypertension, diabetes, cardiovascular disease, liver disease, gallbladder disease, musculoskeletal disorders, and several types of cancer.[1] Quantitative imaging of adipose tissue depots throughout the body could lead to a better understanding of the relationship between obesity and health.[2] Two imaging modalities, x-ray-computed tomography (CT) and magnetic resonance imaging (MRI), are capable of generating quantitative measures of adipose tissue. CT results in a quantitative measure of tissue radiodensity called Hounsfield units (HU), which can detect gradations in adipose tissue properties. The use of CT HU to study adipose tissue is demonstrated in many areas of research such as understanding the lipid content of brown adipose tissue[3] and the change of adipose tissue HU values in growing pigs.[4] MRI is also used to generate quantitative measures of adipose tissue by dividing the MR signal into water and fat components and calculating a quantity called fat signal fraction (FSF). Fat–water MRI (FWMRI) has been extensively studied[5–9] and is accepted as a reliable quantitative method with valuable clinical appliacations.[10–12] Similar to CT HU, MRI-derived FSF values are also sensitive to gradations in adipose tissue quality.

CT can be used to quantify the area and volume of adipose tissue reproducibly,[13] which is correlated with height, weight,[14,15] and waist circumference.[16] In addition to area and volume, it is important to quantify characteristics of adipose tissue such as the radiodensity (CT HU) and fat content (MRI FSF). For example, it has been shown that CT HU measures of adipose tissue are associated with metabolic risk factors such as fasting insulin, blood pressure,[17] hepatic steatosis,[18] and coronary artery disease.[19,20] CT measures of the volume and radiodensity of adipose tissue are positively correlated with body mass index (BMI), with the strongest correlation being between HU and BMI.[21] Although CT has been useful in understanding adipose tissue physiology, it suffers from the use of ionizing radiation, and therefore it is not applicable in all research settings.

MRI is another technique that can be used to quantify the area, volume, and characteristics of adipose tissue noninvasively. Studies have compared adipose tissue area and volume derived using MRI with that derived from CT,[22,23] showing strong agreement between the two modalities. However, unlike CT, MRI does not use ionizing radiation; therefore, it can be used in longitudinal studies and at risk populations such as pediatrics. Furthermore, MRI may provide additional information about adipose tissue structure and function such as FSF. However, MRI measures of adipose tissue characteristics have yet to be correlated with the standard or common CT values.

*Address all correspondence to: E. Brian Welch, E-mail: brian.welch@vanderbilt.edu

2329-4302/2015/$25.00 © 2015 SPIE

Therefore, the purpose of this project is to compare CT HU with MRI-derived FSF in lower abdominal subcutaneous white adipose tissue (WAT). Data presented here were part of a separate study[24] in which subjects underwent two MRI and two PET-CT scans after being exposed to both warm and cold temperatures. The first aim of this work is to determine if the quantitative properties of WAT measured with MRI and CT are self-consistent (intramodality). The second aim assesses intermodality correlation of the quantitative properties of WAT measured by MRI properties to those measured by CT and investigates if this correlation is affected by BMI or temperature.

2 Methods

2.1 *Subjects and Study Setup*

The local ethics committee approved this study to recruit healthy adult subjects to undergo both MRI and PET-CT scans. Data for this study were drawn from a previous study[24] in which 21 subjects (age range: 21.5- to 34.5-years old, BMI range: 20.2 to 31.5 kg/m^2, 8 males, 13 females) were recruited to undergo both MRI and PET-CT scans. Each subject was scanned four times: two PET-CT scans and two MRI scans. The four scans were not acquired in any particular sequence, and each scan was acquired on a separate day. All scans for one subject were acquired within 6 weeks of each other, except for one subject whose scans spanned 5 months. Subjects were asked to refrain from caffeine, alcohol, and strenuous exercise for 24 h prior to the scan day and fast for 8 h prior to arrival for scanning. On the day of the scan, the subjects changed into standardized disposable hospital exam shorts and t-shirts (MediChoice), removing socks and shoes while keeping on underwear. After changing into the standardized clothing, each subject's height and weight were measured using standardized equipment, and BMI was calculated.

The subject sat quietly for 2 h in a temperature-controlled room immediately prior to being scanned. Each of the two PET-CT and MRI scans was performed once after sitting in a warm (24°C) room and once after sitting in a cold (16°C) room. Of the 21 subjects, 18 subjects have a complete dataset consisting of all four scans, two subjects have only cold scan data, and one subject has only warm scan data.

2.2 *Image Acquisition*

MRI scans were acquired on a 3.0 T Philips Achieva MRI scanner (Best, The Netherlands) equipped with two-channel parallel transmit capability. The scans were acquired using an X-tend tabletop (Xtend ApS, Hornslet, Denmark) and a 16-channel Torso-XL surface coil. The FWMRI scans were acquired using a multistack, multislice, multiple fast field echo acquisition with 7 stacks of 20 axial slices, acquired with no gap between slices. Acquisition time was 25 s per stack, with two breath holds performed for each stack. Scanner software was modified to enable the acquisition of eight unipolar echoes (flyback gradients activated) acquired as two time-interleaved sets of four echoes with echo time (TE) values specified as $TE_1 = 1.024$ ms and effective $\Delta TE = 0.779$ ms. Other acquisition protocol details include: repetition time = 83 ms, flip angle = 12 deg, water–fat shift = 0.323 pixels, readout sampling bandwidth = 1346.1 Hz/pixel, axial in-plane field of view = 520 mm × 408 mm, acquired voxel size = 2 mm × 2 mm × 7.5 mm, and sensitivity encoding (SENSE) parallel imaging factor = 3 in the anterior–posterior direction. Also, it is important to note that although T_1 weighting is possible given the scan parameters used, T_1 bias is worst near 50% FSF. Since this work is focused on FSF of WAT, T_1 bias is less of a concern. Specifically, given commonly accepted T_1 relaxation values for water and fat signals along with the sequence parameters used in this work, the estimated maximum absolute and mean absolute bias for FSF greater than 90% are 0.46% and 0.26%, respectively.

PET-CT scans were acquired on a GE Discovery STE PET/CT scanner (General Electric Medical Systems, Milwaukee, Wisconsin). Scans were acquired in helical mode with a 500-mm data collection diameter, a 700-mm reconstruction diameter, a standard convolution kernel, 0.8-s revolution time, and a 1.25-mm single collimation width with a 1.675 spiral pitch factor. Additional scan parameters included: single collimation width = 1.25 mm, total collimation width = 10 mm, source-to-patient distance = 541 mm, source-to-detector = 949.075 mm, and peak kilovoltage = 120 V. Between 299 and 335 slices were acquired, depending on subject height, with a slice thickness of 3.75 mm, and 1.37 mm × 1.37 mm in-plane reconstructed voxel size, and a 512 × 512 matrix size. Scan exposure time lasted 873 s, with an effective dose per CT scan of 3.5 mSv. Acquisition details for both the MRI and PET-CT scans are further explained in our previous publication.[24]

2.3 *Image Processing*

After acquiring the scans, the FWMRI data were separated into water and fat images using a hybrid complex- and magnitude-based method.[25] The complex portion of the fat–water separation was performed using a three-dimensional (3-D) water/fat separation and R_2^* estimation based on a multiscale whole-image optimization algorithm[26] implemented in C++. In this algorithm, fat was modeled using a six-peak spectrum, previously applied across multiple field strengths and anatomies.[27–29] Additionally, the first echo of each four-echo train was discarded to avoid potential contamination by eddy currents in the complex water–fat signal model. Once processed, the FWMRI-derived water and fat images were used to calculate an FSF image by

$$\mathrm{FSF} = \frac{|\mathrm{Fat}|}{|\mathrm{Water}| + |\mathrm{Fat}|}. \quad (1)$$

To process the CT images, the CT DICOM files were loaded into MATLAB (Mathworks Inc., Natick, Massachusetts) and converted to HU by applying the scanner-supplied rescale factors to the data.

Once the images were formed and rescaled, the four scans were coregistered to the same image space for each subject individually. The coregistration was performed with in-house developed three-plane-view software using a rigid body registration algorithm.[30] This registration method ensured registration in all three dimensions. A depot of subcutaneous WAT large enough to obtain measurements without partial volume effects was distinguishable in the posterior lower abdomen of all subjects, even in subjects with the lowest BMI. Therefore, focus was placed on accurate registration of only the lower abdomen to ensure the best registration of the subcutaneous WAT depot. By registering the images prior to further analysis, this not only ensured that the same tissue was being analyzed across scans but also allowed a single mask to be used to extract the subcutaneous WAT region of interest. As part of the

registration process, the MR FSF images were interpolated to the smaller voxel dimensions of the CT images.

All further works to process the images were performed using in-house developed MATLAB scripts. After registration, 10 slices centered at the umbilicus were selected for processing and analysis. To generate the subject-specific subcutaneous WAT mask, the voxels in the 10 slices of the coregistered scans had to fulfill all of the following requirements: MRI FSF values in the range of 85% to 100%, a range set to exclude fascia and include WAT[6,31,32] [e.g., FSF images seen in Figs. 1(a) and 1(d)]; CT HU values in the range of −200 HU to 0 HU, a range known to include WAT[33,34] [e.g., CT images seen in Figs. 1(b) and 1(e)]; and MRI R_2^* values <200 s^{-1},[31,32] to exclude the skin/air interface. These three rules resulted in an initial adipose tissue mask from which the subcutaneous WAT depot was manually selected for each of the 10 slices for every subject. The resulting subcutaneous WAT mask was then further refined on a slice-by-slice basis through a single binary erosion of boundary pixels using the MATLAB function *bwperim* with an eight-connected neighborhood rule to define the perimeter to erode. This perimeter erosion removed small clusters of pixels as well as contracted the boundary of large regions of interest (ROIs), thereby reducing any partial volume effects. Once the final WAT mask was created, statistical comparison showed that the means of the edge voxels and core voxels of each WAT mask were not statistically different for either the FSF or HU values for any subject. This indicated that partial volume effects were absent. These steps resulted in a subject-specific conservative subcutaneous WAT mask. An example slice of the final WAT mask for two subjects is shown in Figs. 1(c) and 1(f). It is important to note that the rigorous segmentation technique applied here may not be practical clinically.

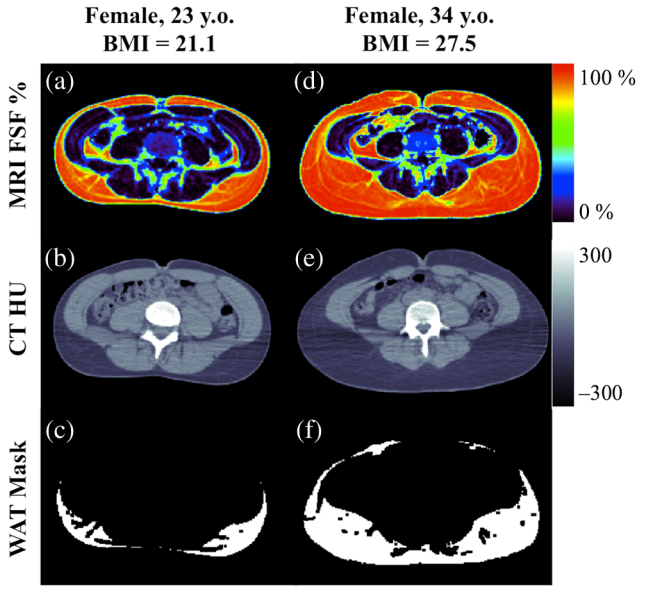

Fig. 1 Axial slices at the umbilicus level of two female subjects: (a)–(c) with a low BMI and (d)–(f) with a high BMI. (a) and (d) The fat–water MRI-derived fat signal fraction (FSF) in percent. The coregistered CT Hounsfield unit (HU) images for each subject are shown in (b) and (e). The corresponding subcutaneous white adipose tissue (WAT) masks are shown in (c) and (f). The rules used to generate the WAT masks are based on FSF and HU values, may exclude fascia, and use boundary erosion to reduce partial volume effects, thereby resulting in a conservative estimate of WAT.

However, by automating region selection and segmentation, this research aims to be reproducible and to reduce the potential subjectivity of manual selection of ROIs.

After creating the subject-specific WAT mask, the mask was applied to the coregistered MRI FSF and CT HU images to obtain the FSF and HU values for each voxel in the masked regions. For each subject, the 10 slices of data were averaged to obtain a single MRI FSF and CT HU value for both the warm and cold conditions. All statistical analyses were performed using RStudio (0.98.1091; RStudio, Inc., Boston, Massachusetts). The FSF and HU values obtained were plotted, and linear regression was performed to determine the correlation (R^2), slope, and intercept. For all significance tests, a p-value <0.05 was considered significant.

3 Results

The subjects were divided into groups based on BMI: All BMI ($n = 21$, 8 male); BMI < 25 kg/m^2 ($n = 15$, 5 male, BMI range: 20.2 to 24.7 kg/m^2); and BMI ≥ 25 kg/m^2 ($n = 6$, 3 male, BMI range: 25.3 to 31.5 kg/m^2). The normal BMI and overweight BMI groups are statistically different from each other ($p < 0.0001$), while the age distributions of the two groups are not statistically significantly different. Dividing the subjects by BMI allows a comparison of data for different BMI levels, as previous groups have shown a correlation of HU values to BMI level.[15,21] Figure 1 shows images from two subjects, one with a low BMI (female, 23 y.o.; BMI = 21.1) and one with a high BMI (female, 34 y.o.; BMI = 27.5). This figure shows for each subject an axial slice of the registered MRI FSF [Figs. 1(a) and 1(d)], CT HU [Figs. 1(b) and 1(e)], and the generated WAT mask [Figs. 1(c) and 1(f)].

To assess the level of correlation using the same imaging modality, the cold values are plotted against the warm values for the same modality. Comparison of FSF values is shown in Fig. 2 and HU values is shown in Fig. 3. In Fig. 2, the plots show that the FSF values are strongly correlated with each other when all subjects are considered as a group [$R^2 = 0.92$, $p < 0.0001$; Fig. 2(a)], with a slope and 95% confidence interval (95% CI) of 0.9 [0.7, 1.0], and y-intercept and 95% CI of 11.5 [−1.6, 24.5]. Plotting only those subjects with BMI < 25 also shows strong correlation [$R^2 = 0.91$, $p < 0.0001$; Fig. 2(b)]; however, when considering the higher BMI subjects alone [Fig. 2(c)], the correlation is barely significant ($R^2 = 0.92$, $p = 0.04$). Figure 3 shows the comparison of cold HU with warm HU values. Plotting all subjects as a single group shows strong correlation between HU temperatures [$R^2 = 0.70$, $p < 0.0001$; Fig. 3(a)], with a slope and 95% CI of 0.9 [0.6, 1.3] and y-intercept with 95% CI of −5.0 [−38.3, 28.3]. Additionally, separating the subjects by BMI results in strong correlation between HU values for the low BMI group [$R^2 = 0.67$, $p < 0.001$; Fig. 3(b)], and no significant correlation for the high BMI group [$R^2 = 0.54$, $p > 0.05$; Fig. 3(c)]. A full listing of the regression slope and y-intercept values and corresponding 95% CI values are in Table 1.

Assessments of the correlation between the properties of adipose tissue as measured by CT HU and MRI FSF values are presented in Figs. 4–6. Initial analysis was performed on both the cold and warm data keeping all the subjects as one group, as plotted in Fig. 4. In this plot, a single subject has two data points, one for the cold data and one for the warm data. This plot shows a significant correlation between the CT HU and MRI FSF values ($R^2 = 0.54$, $p < 0.0001$), with

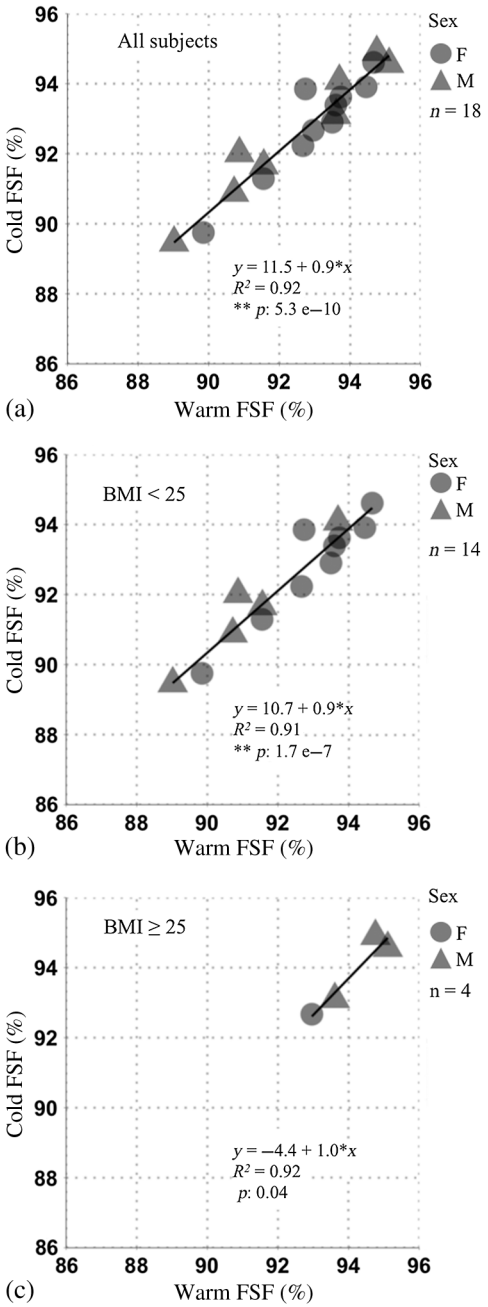

Fig. 2 Plots of the cold and warm fat–water MRI-derived fat signal fraction (FSF) values plotted against each other to investigate the intramodality correlation. (a) The result of plotting all subjects together, (b) the values for the subjects with BMI < 25, and (c) the plot of subjects with a BMI ≥ 25. FSF values are generally self-consistent for all the subjects, showing that for a given value of warm FSF, the corresponding cold FSF is slightly lower. Note that some symbols appear darker because of the overlap of multiple symbols.

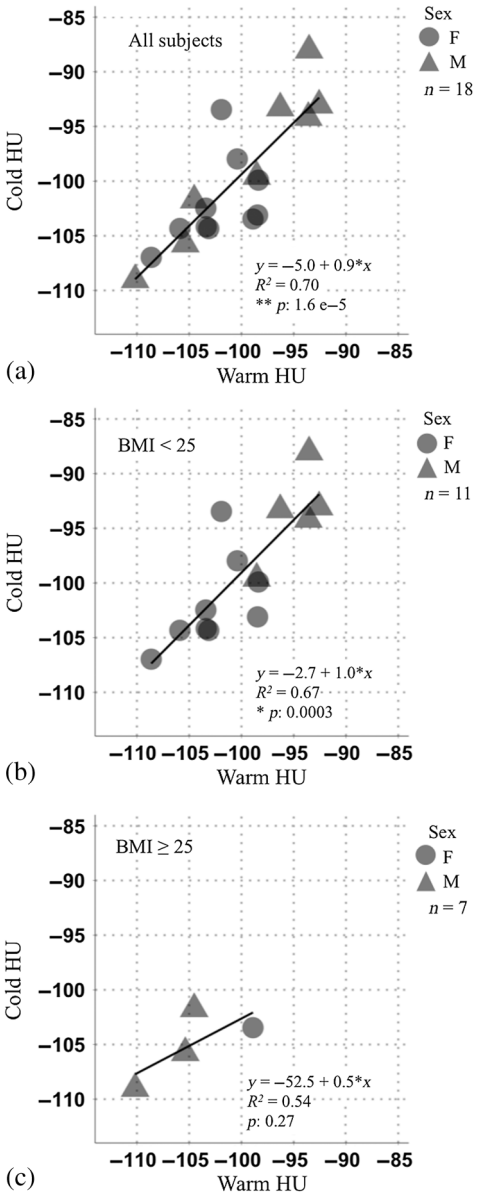

Fig. 3 Plots of the cold and warm CT HU values plotted against each other to investigate the intramodality correlation. (a) The result of plotting all subjects together, (b) the values for the subjects with BMI < 25, and (c) the plot of subjects with a BMI ≥ 25. The HU values of both the plot of all subjects and the subjects with BMI < 25 are self-consistent, whereas for the subjects with BMI ≥ 25 the cold HU values are lower than the warm HU values. Note that some symbols appear darker because of the overlap of multiple symbols.

a slope and 95% CI of −2.6 [−3.3, −1.8], indicating that a change of 1 HU corresponds to a change of 0.38% [0.30%, 0.56%] FSF. Additionally, the y-intercept value and 95% CI of 136.9 [64.1, 209.6] is representative of the HU value expected when the fat content is zero. Comparing the y-intercept value with muscle tissue values (healthy muscle being a tissue with very low fat content), the value of 136.9 is contained within the range of normal muscle attenuation of 30 to 150 HU,[35] and falls far below that of bone.

To investigate any effects of temperature and BMI, the data were split into two ways. First the data were split by BMI, as seen in Figs. 5(a) and 5(b), and then the data were split by temperature, as seen in Figs. 5(c) and 5(d). Grouping the warm and cold data together, but separating the subjects by BMI level, shows that the low BMI data are significantly correlated [$R^2 = 0.52$, $p < 0.0001$; Fig. 5(a)], while the high BMI data are not significantly correlated [$R^2 = 0.32$, $p > 0.05$; Fig. 5(b)]. The results from dividing the data by temperature while keeping all the subjects as one group are plotted in Figs. 5(c) and 5(d). These plots show that both the cold and warm data show significant correlation between the CT HU and the

Table 1 The slope and *y*-intercept values including 95% confidence intervals (CI displayed as [2.5%, 97.5%]) for each plot in Figs. 2–6.

	Slope	*y*-Intercept
FSF versus FSF: ALL BMI	0.9 [0.7, 1.0]	11.5 [−1.6, 24.5]
FSF versus FSF: BMI < 25	0.9 [0.7, 1.1]	10.7 [−5.9, 27.4]
FSF versus FSF: BMI ≥ 25	1.1 [0.1, 2.0]	−4.4 [−94.2, 85.4]
HU versus HU: ALL BMI	0.9 [0.6, 1.3]	−5.0 [−38.3, 28.3]
HU versus HU: BMI < 25	1.0 [0.5, 1.4]	−2.7 [−45.0, 39.5]
HU versus HU: BMI ≥ 25	0.5 [−0.9, 1.9]	−52.5 [−200.3, 95.3]
HU versus FSF: all temp and all BMI	−2.6 [−3.3, −1.8]	136.9 [64.1, 209.6]
HU versus FSF: all temp and BMI < 25	−2.5 [−3.4, −1.5]	127.4 [42.1, 212.7]
HU versus FSF: all temp and BMI ≥ 25	−2.9 [−6.2, 0.5]	164.8 [−152.2, 481.8]
HU versus FSF: warm and all BMI	−2.5 [−3.6, −1.3]	129.5 [21.9, 237.1]
HU versus FSF: cold and all BMI	−2.7 [−3.9, −1.5]	147.1 [35.1, 259.1]
HU versus FSF: warm and BMI < 25	−2.2 [−3.7, −0.7]	105.4 [−31.2, 242.1]
HU versus FSF: warm and BMI ≥ 25	−3.9 [−11.4, −3.6]	262.5 [−447.6, 972.7]
HU versus FSF: cold and BMI < 25	−2.7 [−4.1, −1.4]	154.8 [30.8, 278.7]
HU versus FSF: cold and BMI ≥ 25	−2.3 [−8.6, 4.1]	111.0 [−484.4, 707.8]

MRI FSF values [$R^2 = 0.54$, $p < 0.001$; Fig. 5(d)] than the warm data [$R^2 = 0.54$, $p < 0.001$; Fig. 5(c)].

To further explore how the measure of adipose tissue properties compares between CT HU and MRI FSF, the data were split by both temperature and BMI level, as shown in Fig. 6. Here, the data for the low BMI group show significant correlation both under warm [$R^2 = 0.45$, $p < 0.01$; Fig. 6(a)] and cold [$R^2 = 0.62$, $p < 0.001$; Fig. 6(b)] conditions. The data for the high BMI group do not show significant correlation for either warm [$R^2 = 0.71$, $p > 0.05$; Fig. 6(c)] or cold [$R^2 = 0.20$, $p > 0.05$; Fig. 6(d)] temperatures. The data for the cold low BMI group have the highest R^2 value of 0.62 out of all the groups comparing CT HU and MRI FSF with a mean slope and 95% CI of −2.7 [−4.1, −1.4] and mean *y*-intercept and 95% CI of 154.8 [30.8, 278.7]. A full listing of the regression slope and *y*-intercept values and corresponding 95% CI values for all plots is in Table 1.

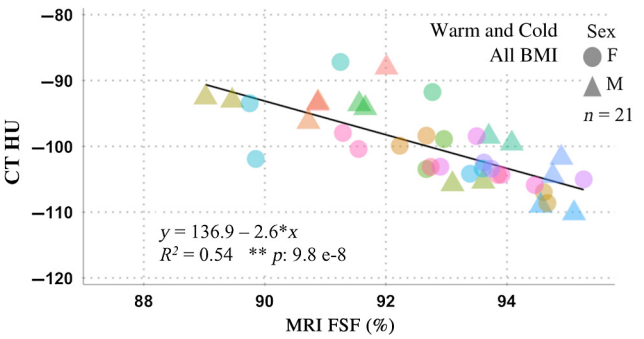

Fig. 4 Plot of CT HU versus fat–water MRI FSF of both the warm and cold data for all 21 subjects. This shows a strong correlation between the HU and FSF measures of abdominal subcutaneous white adipose tissue quality. Note that the same color marker represents the same subject under warm and cold conditions.

4 Discussion

In this study, we measured the properties of abdominal subcutaneous WAT in 21 healthy adults with a range of BMI levels using both CT HU and FWMRI-derived FSF. Both the CT and MRI scans were performed twice for each subject, once after exposing the subject to warm temperatures and once after exposure to cold temperatures. This enabled the values to be compared both intramodality, as well as correlating the two modalities to each other. When comparing intramodality data, both the FSF and HU values demonstrated strong consistency between scans. It is possible that one reason for disagreement is a result of a resonant frequency shift of the water peak due to temperature. This is not accounted for in the FWMRI reconstruction in this study because of insufficient spectral resolution (too few echoes) in the acquired data. Another possibility is that there may be a physiological factor occurring that accounts for the difference in fat measured at the two temperatures. Despite the possibility for physiological differences at the different temperatures, the difference in values for both FSF and HU data is only very slight. Because this dataset does not include two scans at the same temperature, an intramodality comparison could not be made within temperature. Additionally, it should be noted that the fat spectrum model used here has been applied across multiple anatomies and static magnetic field strengths for fat–water separation.[28,29] However, the employed fat spectrum was specifically estimated from human liver. The exact impact of a liver fat spectrum on the

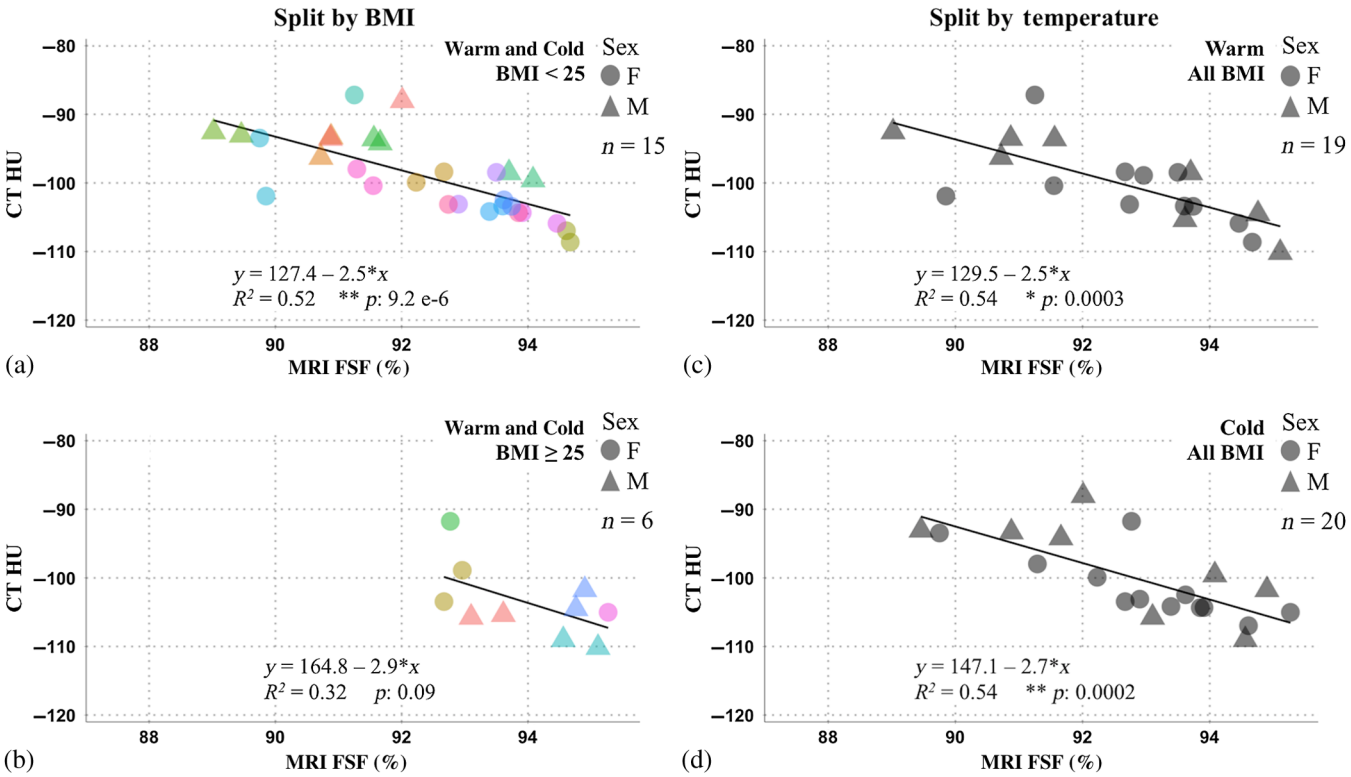

Fig. 5 Separating the entire dataset either by BMI level as seen in (a) and (b) or by temperature as in (c) and (d). Plotting the warm and cold data together shows a strong correlation between CT HU and MRI FSF (a) for the subjects with BMI < 25, (b) but not for subjects with BMI ≥ 25. Splitting all the subjects by temperature results in a correlation between the HU and FSF measures of adipose tissue quality for both (c) warm and (d) cold data. Note that within (a) and (b), the same color marker represents the warm and cold data for one subject. However, the color of the markers is self-contained to each plot.

accuracy of the MRI FSF measurements in subcutaneous WAT presented here is unknown.

After determining that the HU and FSF measures were self-consistent, the two values were correlated to each other. This correlation was first performed disregarding the potential influence of either subject BMI or scan temperature on the measured properties, followed by separating the data by BMI and temperature independently, and finally separating the data by both BMI and temperature. The data were separated by BMI to determine if there was a difference in the subcutaneous WAT quantitative properties based on BMI as has been previously reported. Interestingly, the correlation between the FSF and HU values is strongest for subjects with lower BMI who have been exposed to cold temperatures immediately prior to scanning [Fig. 6(b)]. There are several factors that may explain this connection.

First, it is possible that there is a difference in physiologic response after exposure to cold between the leaner and heavier subjects. The subjects with lower BMI may be more susceptible to cold, while those with higher BMI may have less of a response to the cold and therefore the data will not differ as greatly from their warm data. Cold-induced vasoconstriction causes a redistribution of blood from the periphery to the core, particularly in leaner subjects.[36] Therefore, the SAT may become less perfused with flowing blood in the leaner subjects. Because flowing blood may not be detected fully by FWMRI FSF while still affecting radiodensity measured by CT HU, the cold condition with less blood perfusion is likely a more direct comparison of tissue adiposity between FSF and HU. It is interesting to note that previous work by Kern et al.[37] showed an increase in UCP1 and PGC1α mRNA in the winter compared with the summer from biopsies of subcutaneous abdominal WAT. Although it is likely not the case that the FSF and HU values are picking up on these changes, it is noteworthy that other research also shows differences to the subcutaneous WAT depot due to exposure to cold temperatures. Because these data were acquired as part of a separate study where biopsies were not acquired, histological confirmation of the changes in tissue composition cannot be assessed in this report.

Second, the range of both HU and FSF values is reduced for high BMI subjects compared with subjects with low BMI. The subjects with higher BMI have reduced variability in both HU and FSF values, which can result in weaker correlations because the data are tightly clustered. As seen in Fig. 2, the FSF range for subjects with low BMI is 5.7%, ranging from 89.0% to 94.7% fat, whereas for subjects with high BMI, the FSF range is much smaller at only 2.3%, ranging from 92.6% to 94.9% fat. Similar to the trend of values seen in FSF, the HU range for subjects with low BMI spans a wider range than the HU values of the higher BMI subjects. The low BMI subjects show a range of 20.6 HU (from −108.6 to −88.0 HU), while the subjects with high BMI span only 11.3 HU (from −110.2 to −98.9 HU). The variation in the range of adipose tissue property values for the different levels of BMI is in agreement with previous research showing a correlation between high BMI and lower (more negative) CT

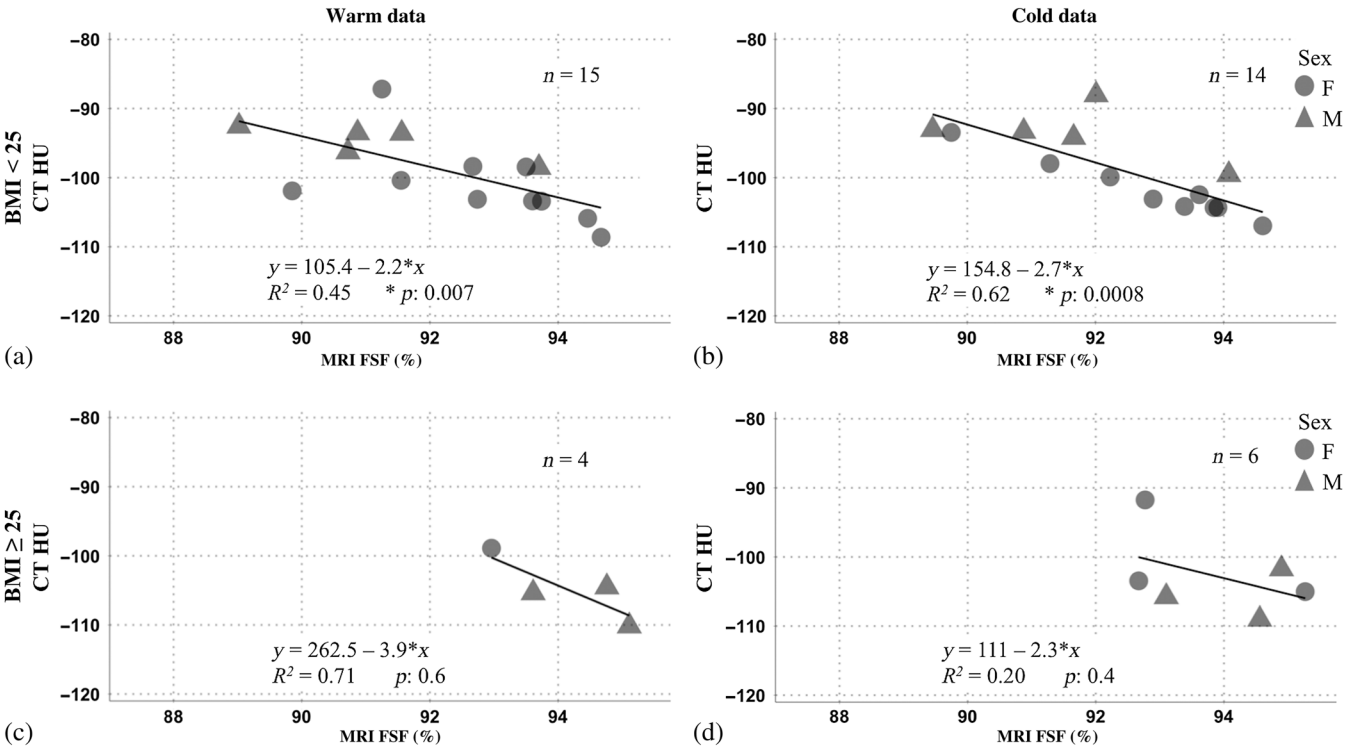

Fig. 6 Plots of the dataset split by both BMI level and scan temperature. This split reveals the strongest correlation between the two measures of adipose tissue quality for the subjects with (b) BMI < 25 exposed to cold. (a) The warm data for subjects with BMI < 25 are also significant, although the correlation is slightly weaker. However, neither (c) the warm nor (d) the cold plots are significantly correlated for subjects with BMI ≥ 25.

HU values.[21] Although it is possible that this broader range of FSF values in the WAT of leaner subjects is due to factors such as cell size,[38–40] without tissue biopsy to confirm we currently do not have an explanation of this observation. This finding warrants further investigation, especially in regards to the connection between FSF and BMI, as this appears to be unexplored in the current literature.

While this study reports promising initial findings in the correlation between MRI FSF and CT HU values, this work suffers from a few limitations. Due to the limited enrollment of overweight subjects in this study, there is not enough power to fully understand the correlation between BMI versus either FSF or HU values. However, because of the connection between BMI and the properties of adipose tissue, this study could be improved by including a wider range of BMI values in a larger cohort. There is also the weakness that this study does not include repeated scans from the same imaging modality under the same temperature. Therefore, intrasubject variability within imaging modality cannot be estimated for this study. However, this study does begin to explore the correlation of MRI-derived FSF of adipose tissue to CT HU and uncovers temperature as a potential factor affecting quantitative measurements of subcutaneous WAT in the lower back. Our findings could also be enhanced by future comparison of FSF with HU values from a multispectral CT unit. This is because measurements from more than one energy level provide additional information about tissue composition that is not available using a single energy source.

In support of reproducible research, the source code along with figure reproduction scripts and data is freely available for download from Ref. 41.

5 Conclusions

This work demonstrates that FSF obtained using quantitative FWMRI at 3.0 T is significantly correlated with CT HU. Additionally, the finding that HU of subcutaneous adipose tissue is inversely related to BMI is supported by the current literature,[21] serving to verify in part, our results. Though the finding of a correlation between CT HU and MRI-derived fat-signal fraction is perhaps not a surprise, little work currently exists in the literature to demonstrate this correlation. The work here shows that given the correlation of MRI FSF to CT HU, FSF could be used as an alternative to CT HU for assessing metabolic risk factors via the impact on adipose tissue quality. Additionally, spatial mapping of quantitative adipose tissue properties, in addition to the assessment of adipose distribution and volume, could enhance understanding of health factors affected by adipose tissue.

Acknowledgments

We would like to thank the volunteers who participated in this study, the MRI and PET-CT technologists for their assistance and expertise in acquiring the scans, as well as our funding sources: R21DK096282 from NIDDK/NIH, UL1 TR000445 from NCATS/NIH, and T32EB014841 from NIBIB/NIH.

References

1. R. H. Eckel et al., "The metabolic syndrome," *Lancet* **375**(9710), 181–183 (2010).
2. H. Wang, Y. E. Chen, and D. T. Eitzman, "Imaging body fat: techniques and cardiometabolic implications," *Arterioscler., Thromb., Vasc. Biol.* **34**(10), 2217–2223 (2014).

3. S. Baba et al., "CT Hounsfield units of brown adipose tissue increase with activation: preclinical and clinical studies," *J. Nucl. Med.* **51**(2), 246–250 (2010).
4. F. J. McEvoy et al., "Hounsfield unit dynamics of adipose tissue and non-adipose soft tissues in growing pigs," *Res. Vet. Sci.* **84**(2), 300–304 (2008).
5. M. Bydder et al., "Relaxation effects in the quantification of fat using gradient echo imaging," *Magn. Reson. Imaging* **26**(3), 347–359 (2008).
6. H. H. Hu et al., "Identification of brown adipose tissue in mice with fat-water IDEAL-MRI," *J. Magn. Reson. Imaging* **31**(5), 1195–1202 (2010).
7. M. Bydder et al., "Constraining the initial phase in water-fat separation," *Magn. Reson. Imaging* **29**(2), 216–221 (2011).
8. E. K. Brodsky et al., "Generalized k-space decomposition with chemical shift correction for non-Cartesian water-fat imaging," *Magn. Reson. Med.* **59**(5), 1151–1164 (2008).
9. H. Yu et al., "Multiecho water-fat separation and simultaneous R_2* estimation with multifrequency fat spectrum modeling," *Magn. Reson. Med.* **60**(5), 1122–1134 (2008).
10. S. Meisamy et al., "Quantification of hepatic steatosis with T1-independent, T2-corrected MR imaging with spectral modeling of fat: blinded comparison with MR spectroscopy," *Radiology* **258**(3), 767–775 (2011).
11. S. B. Reeder and C. B. Sirlin, "Quantification of liver fat with magnetic resonance imaging," *Magn. Reson. Imaging Clin. North Am.* **18**(3), 337–357 (2010).
12. M. Bydder et al., "Assessment of liver fat quantification in the presence of iron," *Magn. Reson. Imaging* **28**(6), 767–776 (2010).
13. P. Maurovich-Horvat et al., "Comparison of anthropometric, area- and volume-based assessment of abdominal subcutaneous and visceral adipose tissue volumes using multi-detector computed tomography," *Int. J. Obes. (Lond.)* **31**, 500–506 (2007).
14. H. Kvist et al., "Total and visceral adipose-tissue volumes derived from measurements with computed tomography in adult men and women: predictive equations," *Am. J. Clin. Nutr.* **48**(6), 1351–1361 (1988).
15. W. O. Grauer et al., "Quantification of body fat distribution in the abdomen using computed tomography," *Am. J. Clin. Nutr.* **39**(4), 631–637 (1984).
16. K. Lee et al., "Waist circumference, dual-energy X-ray absortiometrically measured abdominal adiposity, and computed tomographically derived intra-abdominal fat area on detecting metabolic risk factors in obese women," *Nutrition* **24**, 625–631 (2008).
17. S. R. Smith et al., "Contributions of total body fat, abdominal subcutaneous adipose tissue compartments, and visceral adipose tissue to the metabolic complications of obesity," *Metabolism* **50**, 425–435 (2001).
18. B. J. Park et al., "Visceral adipose tissue area is an independent risk factor for hepatic steatosis," *J. Gastroenterol. Hepatol.* **23**, 900–907 (2008).
19. S. Sarin et al., "Clinical significance of epicardial fat measured using cardiac multislice computed tomography," *Am. J. Cardiol.* **102**, 767–771 (2008).
20. K. Osawa et al., "Nonalcoholic hepatic steatosis is a strong predictor of high-risk coronary-artery plaques as determined by multidetector CT," *PLoS One* **10**(6), e0131138 (2015).
21. K. J. Rosenquist et al., "Visceral and subcutaneous fat quality and cardiometabolic risk," *JACC Cardiovasc. Imaging* **6**(7), 762–771 (2013).
22. J. C. Seidell, C. J. Bakker, and K. van der Kooy, "Imaging techniques for measuring adipose-tissue distribution—a comparison between computed tomography and 1.5-T magnetic resonance," *Am. J. Clin. Nutr.* **51**(6), 953–957 (1990).
23. J. Kullberg et al., "Whole-body adipose tissue analysis: comparison of MRI, CT and dual energy x-ray absorptiometry," *Br. J. Radiol.* **82**(February), 123–130 (2009).
24. A. Gifford et al., "Human brown adipose tissue depots automatically segmented by positron emission tomography/computed tomography and registered magnetic resonance images," *J. Visualized Exp.* (96), e52415 (2015).
25. H. Yu et al., "Combination of complex-based and magnitude-based multiecho water-fat separation for accurate quantification of fat-fraction," *Magn. Reson. Med.* **66**(1), 199–206 (2011).
26. J. Berglund, H. Ahlström, and J. Kullberg, "Model-based mapping of fat unsaturation and chain length by chemical shift imaging-phantom validation and in vivo feasibility," *Magn. Reson. Med.* **68**(6), 1815–1827 (2012).
27. M. S. Middleton et al., "How much fat is under the water peak in liver fat MR spectroscopy?" in *17th Annual Mtg. of ISMRM*, Honolulu, Hawaii, p. 4331 (2009).
28. E. B. Welch et al., "2012 ISMRM challenge on water-fat reconstruction final team standings," International Society of Magnetic Resonance in Medicine, 2012, http://www.ismrm.org/challenge/node/18 (Archived by WebCite at http://www.webcitation.org/6bxOBP0Ql) (1 October 2015).
29. J. Tsao et al., "2012 ISMRM challenge on water-fat reconstruction judging," International Society of Magnetic Resonance in Medicine, 2012, http://www.ismrm.org/challenge/node/17 (Archived by WebCite at http://www.webcitation.org/6bxPUKgNR) (1 October 2015).
30. F. Maes et al., "Multimodality image registration by maximization of mutual information," *IEEE Trans. Med. Imaging* **16**(2), 187–198 (1997).
31. H. H. Hu et al., "Variations in T(2)* and fat content of murine brown and white adipose tissues by chemical-shift MRI," *Magn. Reson. Imaging* **30**(3), 323–329 (2012).
32. H. H. Hu et al., "Characterization of human brown adipose tissue by chemical-shift water-fat MRI," *AJR, Am. J. Roentgenol.* **200**(1), 177–183 (2013).
33. T. Yoshizumi et al., "Abdominal fat: standardized technique for measurement at CT," *Radiology* **211**(1), 283–286 (1999).
34. S. Kim et al., "Body fat measurement in computed tomography image," *Biomed. Sci. Instrum.* **35**, 303–308 (1999).
35. J. Aubrey et al., "Measurement of skeletal muscle radiation attenuation and basis of its biological variation," *Acta Physiol.* **210**(3), 489–497 (2014).
36. S. L. J. Wijers, W. H. M. Saris, and W. D. van Marken Lichtenbelt, "Cold-induced adaptive thermogenesis in lean and obese," *Obesity (Silver Spring)* **18**(6), 1092–1099 (2010).
37. P. A. Kern et al., "The effects of temperature and seasons on subcutaneous white adipose tissue in humans: evidence for thermogenic gene induction," *J. Clin. Endocrinol. Metab.* **99**(12), E2772 (2014).
38. C. Weyer et al., "Enlarged subcutaneous abdominal adipocyte size, but not obesity itself, predicts type II diabetes independent of insulin resistance," *Diabetologia* **43**(12), 1498–1506 (2000).
39. K. C. Hames et al., "Adipose tissue fatty acid storage factors: effects of depot, sex and fat cell size," *Int. J. Obes. (Lond.)* **39**(6), 884–847 (2015).
40. K. L. Spalding et al., "Dynamics of fat cell turnover in humans," *Nature* **453**(7196), 783–787 (2008).
41. https://github.com/gifforda/JMI_Gifford_WAT_CT_HU_vs_MRI_FSF (SHA-1hash=94fb8953280d51317214e2298b82e27d6530abb5).

Aliya Gifford is a PhD candidate in the Chemical and Physical Biology Program at Vanderbilt University in Nashville, Tennessee, USA, under her adviser Dr. E. Brian Welch. She also holds a MS from Virginia Tech in physics and a BS from Randolph Macon Woman's College in physics. Her areas of expertise include MRI characterization of brown adipose tissue as well as compiling, processing and analyzing multi-modality imaging data.

Ronald C. Walker is a professor of Clinical Radiology & Radiological Sciences at Vanderbilt University. His research is focused on molecular imaging of cancer both to improve early and accurate diagnosis and to provide rapid assessment of tumor biology with physiological imaging, and on radiation therapy for cancer based on targeted molecular receptors within or on the cancer cell.

Theodore F. Towse is an assistant professor in the Physical Medicine and Rehabilitation Department at Vanderbilt University. He is interested in the study of skeletal muscle metabolism using non-invasive imaging techniques. He is using this approach to understand muscle dysfunction in patients with neuromuscular conditions such as amyotrophic lateral sclerosis (ALS).

E. Brian Welch is an assistant professor in the Department of Radiology and Radiological Sciences in the Vanderbilt University School of Medicine. His research focuses on overcoming the real world limitations of MRI that hinder research and clinical applications. Additional current research projects include whole-body fat-water MR imaging in both human and animal subjects as well as image acquisitions and reconstructions using non-Cartesian sampling strategies in combination with continuously moving table MRI.